Eur. Phys. J. D **3**, 13–20 (1998)

THE EUROPEAN PHYSICAL JOURNAL D

Sextet levels in the phosphorus-like ion Cu^{14+}

E. Träbert[1,a], S. Fritzsche[2], and C. Jupén[3]

[1] Experimentalphysik III, Ruhr-Universität Bochum, 44780 Bochum, Germany
[2] Fachbereich Physik, Universität Kassel, 34132 Kassel, Germany
[3] Fysiska Institutionen, University of Lund, 22362 Lund, Sweden

Received: 14 April 1998 / Accepted: 18 April 1998

Abstract. Delayed spectra of foil-excited fast Cu ions have been studied to find a number of $3s3p^4$, $3s^23p^23d$ and $3s3p^33d$ levels in the P-like ion Cu^{14+} (spectrum Cu XV). Among these are $3s3p^33d\ ^6D$ levels, which have never been observed before, although they are the lowest excited states that have the same parity as the ground configuration. The investigation combined theory and experiment. The calculations used the Cowan code with semi-empirically scaled parameters and extensive MCDF computations.

PACS. 32.30.Jc Visible and ultraviolet spectra – 31.50.+w Excited states – 32.70.Fw Absolute and relative intensities

1 Introduction

In 1941 and since, Edlén [1–3] showed that many of the unidentified lines in the spectrum of the solar corona corresponded to electric-dipole-"forbidden" magnetic dipole (M1) transitions within the ground configurations $3s^23p^k$ ($k = 1 - 5$) of highly charged Fe and Ni. This identification changed our views of the solar corona, because in order to produce such highly charged ion species, temperatures in the corona must be much higher than that of the photosphere, the visible solar surface. The same forbidden transitions have since been used for the diagnostics of hot laboratory plasmas. A detailed knowledge of the atomic structure of the highly charged, but only partially ionized, atoms is needed to model and understand radiative transport in solar and terrestrial plasmas.

Nowadays, massive computer algorithms help to predict atomic structure of many-electron systems to often better than 1% of the gross structure. However, the relative uncertainties of calculated term differences are generally much larger, and therefore it is difficult to predict transition wavelengths with a precision sufficient to make spectroscopic classification simple. Checking available experimental data on highly charged atoms of iron group elements [4–15] shows a data base which - although in the process of improvement - is still grossly incomplete: Many ground state transitions in highly charged ions of the iron period elements up to Ni are known, and thus the ground complex fine structure intervals are well established. However, many levels of the first excited electron configurations (mostly $3p - 3d$ excitation) are not yet known, in particular those with a high total angular momentum quantum number, which cannot decay to the ground complex by electric dipole (E1) decay.

For example, in the P I isoelectronic sequence, the ground configuration is $3s^23p^3$, with a $^4S^o$ ground state. Although in the ground complex there are both doublet and quartet terms, theory predicts intercombination transitions to appear: The $3s^23p^23d\ ^4D$, ^4F levels with $J > 5/2$ cannot decay to the $3s^23p^3\ ^4S^o_{3/2}$ level by E1 transitions. The decay of the $J = 7/2$ levels instead leads to the $3s^23p^3\ ^2D^o_{5/2}$ level, and the $J = 9/2$ level lives even longer as its only decay is *via* a forbidden (M1/E2) transition to the $J = 7/2$ levels of the same configuration. Such M1 transitions in excited configurations are candidates for identification with some coronal lines found in the recent SOHO spectra [16]. Predicted lifetimes of most such $J = 7/2$ levels are of the order of 10 ns and higher (The decay of one short-lived J=7/2 level has been seen in earlier beam-foil work [5] as well as in the laser-produced plasma studied by Sugar and Kaufman [9]). Such long-lived levels would likely be quenched by collisions in most terrestrial plasmas, but the corresponding spectral lines may be expected to be seen in beam-foil spectra recorded with a sufficiently long delay after excitation. In fact, some of the ground state transitions from long-lived $J = 7/2$ levels have recently been identified [17] in delayed spectra of foil-excited fast ion beams [18–23,17], guided by semi-empirically adjusted Multi-Configuration Hartree-Fock (MCHF) calculations [24] as implemented in the Cowan code [25].

These high-J levels are not the only long-lived ones, however. The $3s3p^33d$ configuration can form sextet ($^6D^o$) levels, which can only decay by intercombination transition, to either the $3s3p^4\ ^4P$ or the $3s^23p^23d\ ^4L$ levels,

[a] e-mail: traebert@EP3.ruhr-uni-bochum.de

but not to the ground state (because of the same parity). Unfortunately, the intensities of most transitions will be low, because several decay branches exist. The strongest lines expected are $3s^23p^23d\ ^4F_{7/2,9/2}$ - $3s3p^33d\ ^6D^o_{7/2,9/2}$, of which neither the lower nor the upper levels have been observed before. The corresponding wavelengths are predicted near 40 nm for Cu.

In the present study we aim at identifying transitions from these lowest excited levels. This will test our present understanding of the atomic structure of such rather high excited levels. In typical structure calculations, levels of a given parity are grouped and evaluated together, because they interact. However, there are so many excited states, and so many electron configurations that might play a role, that some limitations need to be introduced for this first step. We therefore concentrate on the $3s3p^33d\ ^6D$ levels in P-like ions, for various reasons: Firstly, the ^6D term has the lowest excited levels of the same parity as the $3s^23p^3$ ground state (with terms $^4S^o$, $^2P^o$, and $^2D^o$), and it seems well separated in energy from other excited levels. This helps to isolate in wavelength range the prospective decays to $3s^23p^23d$ and $3s3p^4$ levels. Secondly, the high spin of the upper level necessitates a spin change in any decay, because there are no lower sextet levels, and therefore reduces the number of possible decay channels considerably. Thirdly, the spin-changing (intercombination) transitions with their lower transition probabilities result in longer lifetimes of the upper levels than would be the case with fully allowed decays. Levels of longer lifetime can be (relatively) enhanced in delayed spectra [18,20,26].

The present study continues the multi-element beam-foil studies of the extreme-ultraviolet (EUV) spectral range presented elsewhere [27,20,21,23,17]. Although the wavelength measurement precision in such beam-foil work is regularly inferior to that available from bright, stationary light sources, foil-excited fast ion beams have advantages for the present type of study [26]:

- the fast ion beam is isotopically pure, and the charge state distribution can be varied in a controlled, roughly predictable manner,
- by recording time resolved spectra shortly after excitation or after some (few ns) delay, decays of long-lived levels can be identified as such, and in many cases (rough) atomic level lifetime values be obtained,
- with an optically thin light source and an efficiency-calibrated spectrometer, intensity patterns of line multiplets can be used to determine branching ratios, and
- with a combination of simulated time-resolved spectra based on theoretical data and experimental atomic data (wavelength, apparent lifetime, relative intensity), various parameters of theoretical models can be checked against experimental evidence, and the calculation with the best predictive power be selected for those systems not covered by the actual experiment.

We note, however, that the experimental data base for elements beyond Ni ($Z = 28$) is markedly poorer than for the elements up to Ni. For example (according to the latest compilations [11,14,15]), in Cu XV the five levels of the ground configuration $3s^23p^3$ are known experimentally, two out of 8 levels of the configuration $3s3p^4$, and 9 out of 28 levels of the $3s^23p^23d$ configuration. This lack of completeness is partly caused by the fact that the pioneering EUV study on highly charged Cu [9] was done with a laser-produced plasma which quenches long-lived levels, and neither this work nor subsequent work on a tokamak plasma [10,12] covered the wavelength range of the $3s3p^4$ level decays. These data and some new experimental data from our own beam-foil work are to be compared with extensive Multi-Configuration Dirac-Fock (MCDF) calculations (see also work on the Cl sequence [28]) which, for the P-like ion Cu^{14+}, have been extended beyond the status reached for other P-like ions [29]. An earlier MCDF calculation, by Huang [30], included a number of configurations beyond that of the ground state in the computation, but did not present results on any odd-parity excited levels.

2 Calculation

In order to guide the experimental search, Cowan code calculations with standard values of the Slater parameters [25] were done. These calculations indicated the wavelength ranges of the more prominent decay branches of the wanted $3s3p^33d\ ^6D$ levels as well as lifetimes and branching ratios (needed for the simulation of spectra). The calculations also showed that most levels have several decay branches of about equal strength, thus distributing the available intensity over several lines (and making each of them more difficult to observe). The individual lifetime predictions varied considerably with the number of configurations used in the calculation, clearly pointing out the need for large-scale computations if reliable predictions were to be gained.

These semi-empirical calculations were good enough, though, to help assign lines from several high$-J$ levels into the lower configurations of P–like ions [17], as did some MCDF calculations of the $3s^23p^23d$ levels [29]. The latter computations came much closer to experiment than those carried out by Huang [30], probably due to a more appropriate size of the wave function expansion.

In the present study, we made a further improvement by including also the rearrangement of the electron cloud during the de-excitation. This was achieved by a separate optimization of the initial and final state wave functions of the different transitions. The incorporation of these "relaxation effects" does not only result in slightly better transition energies but, even more important, in improved theoretical transition probabilities and lifetimes.

To calculate transition probabilities, we applied multiconfiguration Dirac–Fock (MCDF) wavefunctions of a rather extensive size. Since this model of multi–electron atoms and ions is now well established for this kind of studies, we will give only a brief account on theory. For further details on the MCDF method we refer to Grant [31].

In the MCDF model, an atomic state is approximated by a linear combination of configuration state

functions (CSF)

$$\psi_\alpha(PJM) = \sum_{r=1}^{n_c} c_r(\alpha)\,|\gamma_r PJM\rangle\ , \qquad (1)$$

of the same symmetry as labeled by the three quantum numbers PJM of the total parity and angular momentum. In expansion (1), n_c denotes the total number of CSF in the wave functions representation; each of these CSF is built from antisymmetrized products of a common set of Dirac orbitals. These orbitals are traditionally optimized on the basis of the Dirac–Coulomb Hamiltonian [32]. Further relativistic contributions due to the Breit interactions among the electrons and an estimate of the QED corrections are then added later as perturbations. For the computation of the transition matrix, the mixing coefficients $\{c_r(\alpha)\}$ in the wave function expansion were obtained by diagonalizing the Dirac–Coulomb–Breit matrix.

We generated the configuration lists for the $3s^23p^3$ ground state levels and those for the different symmetries of the low–excited $3s^23p^23d$, $3s^23p^24s$, and $3s3p^33d$ levels by applying the active-space method [32,33]. Hereby, a list of CSF for a given parity and angular momentum is obtained by exciting the electrons from one or more reference configurations within an *active set* of subshells. In recent years, such a systematic approach involving a rather large set of subshells has often successfully been applied, in particular for light elements with a simple shell structure [34]. By studying the convergence behaviour of individual properties, a systematic enlargement of the number of orbitals (and, thus, of the active space) then even enables estimates of the accuracy of the theoretical data. For more complex ions, however, as given here by the ions of the phosphorus sequence, the active space method still provides a *systematic* approach, but the five valence electrons outside the $1s^22s^22p^6$ core do not allow to show convergence of individual probabilities and lifetimes. Therefore, to estimate the accuracy of our theoretical data, comparison with experiment is needed.

In the present computations, the active set of orbitals include all subshells with principal quantum numbers $n \le 4$. For this active set, we accounted for all possible excitations (up to quadrupoles) within the $3l$ subshells as well as single (S) and double (D) excitations into the $4l$ shells (keeping the neon–like core closed). Such an active space with SD excitations of the valence electrons up to the $4l$ *layer* then yields a wave functions expansion of a maximum of up to 3698 CSF for the $J = 5/2$ levels. Even though this is a somewhat smaller wave function expansion than applied previously [29], two essential improvements have been made: (i) An independent set of orbitals has been optimized for all five ground–state levels together as well as for each symmetry of excited levels having the same total angular momentum J. Also, the levels from the upper sextet, ^6D_J, have been optimized on an independent orbital basis. (ii) The electron relaxation has been fully included in the computation of the transition matrix [35] by using an extension to GRASP92 which has recently been developed [36]. The transition matrix was then calculated (relativistically) in both, Babushkin and Coulomb, gauges; in non–relativistic notation these gauges are better known as the length and velocity forms of the transition matrix elements. Results in both gauge forms will be shown below.

Section 5 discusses and compares the results of these extended computations along with experimental data. We present level energies and lifetimes and will estimate the accuracy of the data by comparison with measured values.

3 Experiment

The experiment was done as part of an ongoing study at the Bochum Dynamitron Tandem Laboratory (DTL), where a 4 MV tandem accelerator equipped with a Middleton-type, high-current ion source is available. Ion beams of Mn, Fe, Co, Ni, Cu, and Zn were obtained; the individual energies were chosen in the range 7 to 32 MeV in order to optimize the production of ions in particular ionization stages by ion-foil interaction [37,38] with carbon foils of typically 20 μg/cm^2 areal density. In addition to data from the aforementioned studies which concentrated on Mg- to Si-like ions [20,21] as well as S- and Cl-like ions [22,23], spectra were recorded over spectral regions as indicated by calculations (see above), and at ion energies optimum for the production of P-like ions Ni (20 - 28 MeV) and Cu (28 - 29 MeV). These two elements yield particularly high beam currents, which is prerogative in order to optimize the expected weak signal.

The EUV light emitted after foil-excitation was observed by means of a 2.2 m grazing-incidence spectrometer equipped with a channeltron as the detector. The scanning motion of the spectrometer was monitored by a moiré fringe length gauge. The foil could be displaced by up to 17.5 cm to permit the recording of decay curves and of delayed spectra up to times after excitation of order 20 ns. The signal was normalized to the charge collected on a Faraday cup. All wavelength calibrations were of the in-beam type, referring to known lines emitted by fast ion beams and correcting for first and second order Doppler shifts. Decay curves were recorded on a number of spectral lines. For those related to the decays of short-lived levels, the spatial resolution of the spectrometer was taken into account [39]. Details of the set-up and of the data collection and evaluation procedures have been published in earlier papers ([18,20] and Refs. therein).

4 Data and evaluation

Figure 1 gives examples of spectra recorded at different ion energies, so that spectral lines can be identified with ionic charge states, and optimum energies for specific observations can be chosen. Figure 2 covers the wavelength range of the Cu XV $3s^23p^3$ - $3s3p^4$ transitions, figure 3 that of the strongest of the $3s^23p^23d\ ^4L$ - $3s3p^33d\ ^6D$ transitions. The spectral range of Figure 2 has been covered before [5], but not at optimum conditions to single out the $3s3p^4$ decays: Near the foil, the density of lines is often too high to

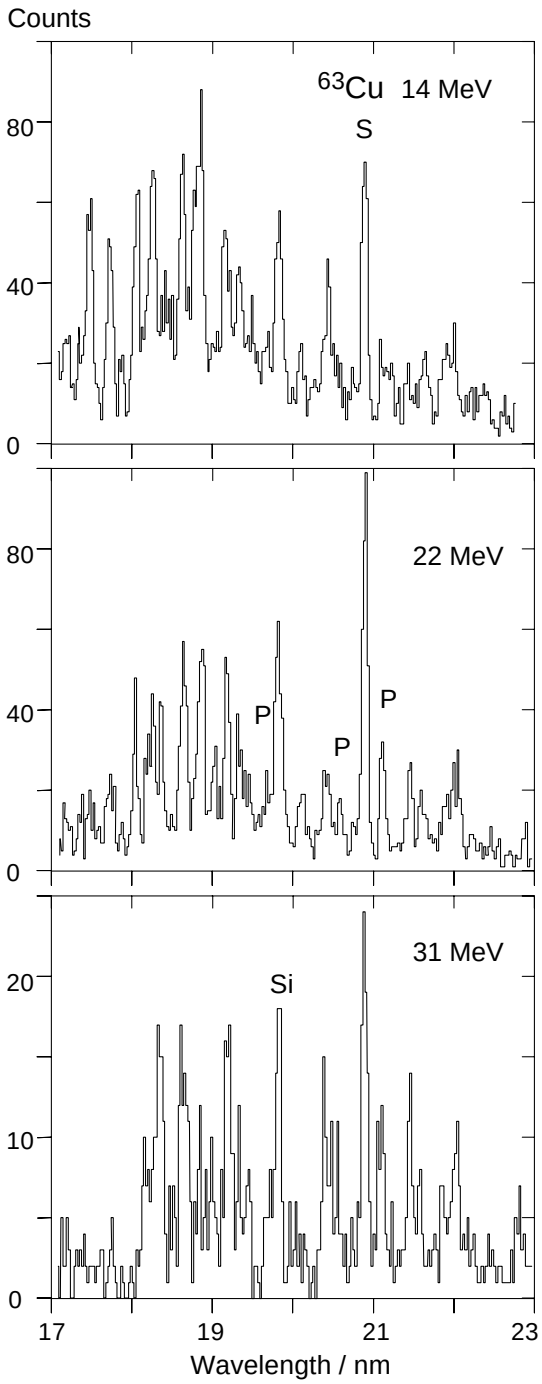

Fig. 1. Delayed spectra of Cu observed at three ion energies. The delay of about 2 ns is the same for all spectra. The isoelectronic sequence labels at some lines identify the following transitions: Si: Cu XVI $3s^2 3p^2\ ^3P_2$ - $3s^2 3p 3d\ ^3F_3$, P: Cu XV $3s^2 3p^3\ ^2D_{5/2}$ - $3s^2 3p^2 3d\ J = 7/2$, S: Cu XIV $3s^2 3p^4\ ^3P$ - $3s^2 3p^3 3d\ ^5P^o$.

identify individual lines, and at a delay-time of about 1 ns, these particular levels with their lifetimes in the 100 ps range yield no clear signal any longer.

The sextet decays of interest have not been observed before. They will be much weaker than the resonance lines because of several factors: Higher-lying levels are generally less populated than low-lying ones. We work with

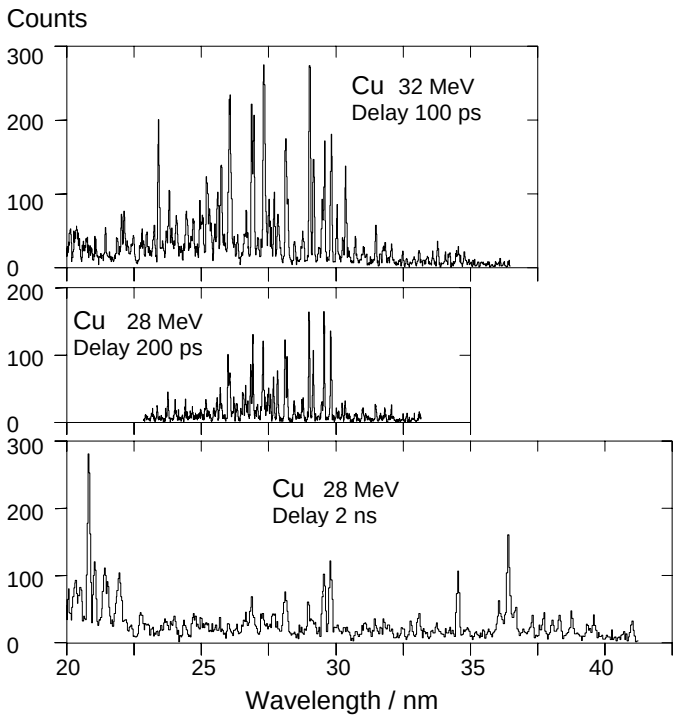

Fig. 2. Spectra of 32 MeV and 28 MeV Cu observed (a) 1 mm downstream of the foil (delay about 100 ps, best for calibration with short-lived level decays in Cu XIX and Cu XVIII), (b) 2 mm downstream of the foil (delay about 200 ps), and (c) 2 cm downstream (2 ns after excitation). At each position, the time interval observed (defined by the field-of-view of the detection system and the ion velocity) is about 100 ps long. These spectra contain the $3s^2 3p^3$ - $3s 3p^4$ transitions of Cu XV.

time-resolved observation; The field of view (0.9 mm wide, corresponding to about 100 ps time-of-flight of the fast ions) is about two orders of magnitude less than the decay lengths of the sextet levels with their (calculated) lifetimes of 4 to 30 ns. For the resonance levels, in contrast, the field of view is much larger than the corresponding decay length. Furthermore, the detection efficiency of the spectrometer set-up in the 40 nm range is lower than in the resonance line wavelength range near 18 nm by about a factor of two [40]. In the predicted wavelength range, there are a number of other lines, mostly from shorter-lived levels. Their relative intensities can be reduced more than those of the lines of interest by observation farther away from the exciter foil (and thus later after excitation). Considering the uncertainty of the prediction (transitions between calculated levels, each of which may be uncertain by a few percent), a range of spectral search of a few nm, near wavelengths of order 40 nm, was to be carried out. In order to produce a signal that exceeded the (low) detector dark rate, μA ion currents (0.5 μA particle currents) were required, which the exciter foils can suffer before breaking for an hour at best. Combining these conditions and requirements, only moderate spectral resolution could be expected. Therefore delayed spectra were recorded with 80 to 150 μm wide slits (line widths (FWHM) 0.06 to 0.12 nm).

Table 1. Observed lines of selected transition arrays in Cu XV. The three arrays lie in different parts of the spectrum which have to be calibrated in different ways. Wavelengths without error bars relate to lines which by position and relative intensity in the simulated spectra are compatible with the observed spectra, but which in the latter are not individually resolved and measured. bl denotes blends with lines other than Cu XV.

Transition	λ (nm)	Reference
$3s^2 3p^3$ – $3s^2 3p^2 3d$		
$^2D^o_{5/2}$ - (^3P) $3d$ $^2G_{7/2}$	18.22 ± 0.02	[17]
$^2D^o_{3/2}$ - (^3P) $3d$ $^4D_{3/2}$	20.08	
$^2D^o_{3/2}$ - (^3P) $3d$ $^4D_{1/2}$	20.14	
$^2D^o_{5/2}$ - (^3P) $3d$ $^4D_{5/2}$	20.16	
$^2D^o_{5/2}$ - (^1D) $3d$ $^2F_{7/2}$	20.63 ± 0.02	[17]
$^2D^o_{5/2}$ - (^3P) $3d$ $^4F_{7/2}$	21.16 ± 0.02	[17]
$^2D^o_{3/2}$ - (^3P) $3d$ $^4F_{3/2}$	21.50	
$^2D^o_{5/2}$ - (^3P) $3d$ $^4F_{5/2}$	21.64	
$^2D^o_{3/2}$ - (^3P) $3d$ $^4D_{1/2}$	22.80	
$3s^2 3p^3$ – $3s3p^4$		
$^2D^o_{3/2}$ - $^2P_{1/2}$	22.98 ± 0.01	
$^2D^o_{5/2}$ - $^2P_{3/2}$	23.81 ± 0.01	
$^2P^o_{3/2}$ - $^2S_{1/2}$	24.70 ± 0.01	
$^2P^o_{1/2}$ - $^2P_{1/2}$	25.49 ± 0.02	
$^2D^o_{3/2}$ - $^2D_{3/2}$	26.96 ± 0.02 bl	
$^2D^o_{5/2}$ - $^2D_{5/2}$	27.34 ± 0.02	
$^4S^o_{3/2}$ - $^4P_{1/2}$	27.71 ± 0.02 bl	
$^4S^o_{3/2}$ - $^4P_{3/2}$	28.16 ± 0.01 bl	
$^4S^o_{3/2}$ - $^4P_{5/2}$	29.59 ± 0.01	
$^2P^o_{3/2}$ - $^2D_{5/2}$	31.50 ± 0.01	
$3s^2 3p^2$ (^3P) $3d$ - $3s3p^3 3d$		
$^4F_{5/2}$ - $^6D^o_{5/2}$	39.29 bl	
$^4F_{5/2}$ - $^6D^o_{7/2}$	39.46 bl	
$^4F_{7/2}$ - $^6D^o_{9/2}$	40.85 ± 0.02 bl	
$^4F_{7/2}$ - $^6D^o_{7/2}$	41.15 ± 0.02 bl	
$^4F_{9/2}$ - $^6D^o_{9/2}$	42.92 ± 0.02 bl	

To enease the identification of lines by visual pattern recognition, spectra were simulated from experimental and calculated data, expecting that line multiplets with a distinctive pattern of relative line intensities and wavelength spacings would be better for identification than individual lines in only partly classified spectra. The simulation of such spectra requires term differences (level energies), transition probabilities and, for lack of experimental data, a model of the initial level populations. For levels of comparable excitation energies, we assumed a statistical population, that is one proportional to the weight factors $2J + 1$.

5 Results and discussion

Spectra near the foil ("prompt") showed many prominent lines, and among them resonance lines of the P-like ions. These lines can be calibrated in high-energy spectra (which were of lower signal because of the accelerator technical limits) with lines in Cu XIX, Cu XVIII and Cu XVI. In particular the Cu XVI transition $3s^2 3p^2\ ^3P_2$ - $3s3p^3\ ^3D^o_3$ at 29.8162 nm [15] is useful, because it can be found in spectra with delays up to 2 ns. A decay curve of this line reveals a mean life of $(520 \pm 30]$ ps, which is in reasonable agreement with an extrapolation of theoretical data for Ni XV [41]. Its neighbouring line is the transition Cu XV $3s^2 3p^3\ ^4S^o_{3/2}$ - $3s3p^4\ ^4P_{5/2}$, for which the decay curve yields a lifetime of (423 ± 25) ps in agreement with our calculational prediction of 436 ps. Both lines show fast and slow cascades, which were treated approximatively by one exponential fit component each. The wavelength of this Cu XV line has earlier been determined as 29.66 nm [5]. We now find this line at (29.59 ± 0.01) nm, and similarly in the recalibrated data used for reference [5]. The other two lines of this multiplet are partially blended, as is true for quite a number of lines of the $3s^2 3p^3$ – $3s3p^4$ transition array (Tab. 1).

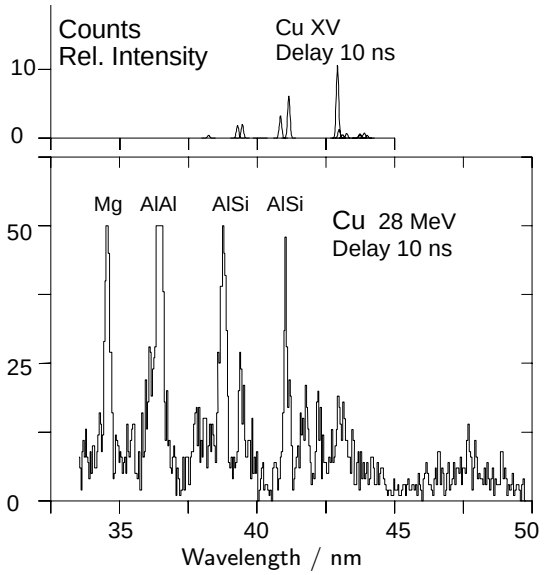

Fig. 3. Measured and simulated delayed (10 ns) detail spectra of Cu XV. Intercombination transitions in Mg-, Al- and Si-like ions of Cu [18] are identified by isoelectronic sequence labels. The simulation of Cu XV uses energies and lifetimes as calculated for this work and contains the strongest of the $3s^2 3p^2 3d\ ^4F$ - $3s3p^3 3d\ ^6D$ transitions. The intensity scale of the simulated spectrum matches that of the experimental data. The excitation energies of the lower levels are from experiment or from educated guesses oriented at measured levels of the same level multiplet. The upper level energies are from our MCDF calculation. The comparison with experimental data shows an almost perfect agreement with the best of several possible matches of measured and simulated spectra. Most of the sextet level decays are blended by other, as yet unidentified lines. At 41.035 nm, for example, the blend is with two intercombination lines of Cu XVI (Si-like) and Cu XVII (Al-like) [18].

Table 2. Cu XV levels calculated with MCDF wavefunctions including SD excitations into the $4l$ layer and data determined by experiment. The levels are ordered by increasing (calculated) excitation energy as in the systematic calculations of several elements [29]. Note that level 19 lies higher than level 20, and level 37 higher than level 38, in the present computation. Explanation of columns: "No." is a running index. "LS-label" level designations are carried over from low-Z ions; however, the labels, in particular the core couplings, are not unequivocal. Explanation of symbols: † M1 rate dominates, ^{a} reference [12], * this work, $^{(*)}$ suggested data from this work: calculated values adjusted, where possible, for the estimated difference between calculated and measured energies, if at least one member of the level multiplet is known. For the sextet levels, the calculated level values are assumed as valid, as they fit to the spectrum, albeit with all lines being blended. The associated uncertainty includes that of the lower level of the transition.

		Theory				Experiment	
		Energy	Lifetime (s)		LS-Label	Energy	Ref.
No.	J	(cm^{-1})	Length	Velocity		(cm^{-1})	
1	3/2	0			$3s^2 3p^3\ ^4S^o$		
2	3/2	49452			$3s^2 3p^3\ ^2D^o$	47940	a
3	5/2	59202			$3s^2 3p^3\ ^2D^o$	57803	a
4	1/2	93129			$3s^2 3p^3\ ^2P^o$	91106	a
5	3/2	107829			$3s^2 3p^3\ ^2P^o$	105962	a
6	5/2	339460	4.36(–10)	4.29(–10)	$3s3p^4\ ^4P$	337100	a
						337950 ± 120	*
7	3/2	356732	3.87(–10)	3.96(–10)	$3s3p^4\ ^4P$	355180 ± 150	*
8	1/2	363451	3.57(–10)	3.69(–10)	$3s3p^4\ ^4P$	360880 ± 250	*
9	3/2	421739	1.86(–10)	1.89(–10)	$3s3p^4\ ^2D$	418860 ± 250	*
10	5/2	426603	2.18(–10)	2.15(–10)	$3s3p^4\ ^2D$	423450 ± 100	*
11	3/2	481056	8.40(–11)	8.32(–11)	$3s3p^4\ ^2P$	477800	a
						477740 ± 200	*
12	1/2	487181	6.82(–11)	6.71(–11)	$3s3p^4\ ^2P$	483200 ± 200	*
13	1/2	514408	9.28(–11)	9.09(–10)	$3s3p^4\ ^2S$	510840 ± 150	*
14	3/2	516982	1.56(–9)	1.47(–9)	$3s^2 3p^2(^3P)3d\ ^4F$	513000	(*)
15	5/2	524009	2.77(–9)	2.64(–9)	$3s^2 3p^2(^3P)3d\ ^4F$	520000	(*)
16	7/2	534308	1.83(–8)	1.82(–8)	$3s^2 3p^2(^3P)3d\ ^2F$	530390 ± 450	*
17	5/2	539184	3.57(–9)	3.42(–9)	$3s^2 3p^2(^1D)3d\ ^2F$	535000	(*)
18	9/2	546175	2.46(–2)	$2.46(-2)^{\dagger}$	$3s^2 3p^2(^3P)3d\ ^4F$	542200	(*)
19	1/2	547487	4.92(–10)	4.76(–10)	$3s^2 3p^2(^3P)3d\ ^4D$	544500	(*)
20	7/2	546765	1.37(–8)	1.24(–8)	$3s^2 3p^2(^1D)3d\ ^4F$	542530 ± 500	*
21	3/2	548913	5.33(–10)	5.11(–10)	$3s^2 3p^2(^3P)3d\ ^4D$	545900	(*)
22	5/2	556900	7.71(–10)	7.40(–10)	$3s^2 3p^2(^3P)3d\ ^4D$	553900	(*)
23	7/2	573766	1.14(–7)	1.45(–7)	$3s^2 3p^2(^3P)3d\ ^4D$	570800	(*)
24	7/2	607270	1.34(–9)	1.28(–9)	$3s^2 3p^2(^1D)3d\ ^2$G	606650 ± 600	*
25	9/2	613575	2.88(–3)	$2.87(-3)^{\dagger}$	$3s^2 3p^2(^1D)3d\ ^2$G	613000	(*)
26	3/2	616070	1.08(–11)	1.03(–11)	$3s^2 3p^2(^1D)3d\ ^2P$	611000	(*)
27	5/2	626589	9.09(–12)	8.69(–12)	$3s^2 3p^2(^3P)3d\ ^4P$	619652	a
28	3/2	633243	9.41(–12)	9.02(–12)	$3s^2 3p^2(^3P)3d\ ^4P$	626264	a
29	1/2	634857	9.81(–12)	9.43(–12)	$3s^2 3p^2(^3P)3d\ ^4P$	633300	a
30	1/2	641375	9.05(–12)	8.70(–12)	$3s^2 3p^2(^1D)3d\ ^2P$	636000	(*)
31	3/2	644766	3.44(–11)	3.30(–11)	$3s^2 3p^2(^1D)3d\ ^2D$	639000	(*)
32	5/2	663075	1.79(–11)	1.71(–11)	$3s^2 3p^2(^1D)3d\ ^2D$	658000	(*)
33	3/2	680946	9.87(–12)	9.50(–12)	$3s^2 3p^2(^3P)3d\ ^2D$	675651	a
34	5/2	682845	1.94(–11)	1.87(–11)	$3s^2 3p^2(^3P)3d\ ^2D$	672380	a
35	1/2	697492	1.13(–11)	1.10(–11)	$3s^2 3p^2(^1D)3d\ ^2$S	687500	(*)
36	5/2	704078	7.47(–12)	7.26(–12)	$3s^2 3p^2(^1D)3d\ ^2F$	704078	(*)
37	1/2	715283	1.07(–11)	1.04(–11)	$3s^2 3p^2(^1D)3d\ ^2P$	706300	(*)
38	3/2	712475	1.08(–11)	1.05(–11)	$3s^2 3p^2(^1D)3d\ ^2P$	703573	a
39	7/2	713718	7.52(–12)	7.29(–12)	$3s^2 3p^2(^1D)3d\ ^2F$	704207	a
40	5/2	744908	8.35(–12)	8.14(–12)	$3s^2 3p^2(^3P)3d\ ^2D$	735639	a
41	3/2	745712	8.65(–12)	8.44(–12)	$3s^2 3p^2(^3P)3d\ ^2D$	735114	a
42	1/2	773172	9.50(–9)	8.75(–9)	$3s3p^3 3d\ ^6D^o$	773172	(*)
43	3/2	773696	9.54(–9)	8.99(–9)	$3s3p^3 3d\ ^6D^o$	773696	(*)
44	5/2	774513	1.29(–8)	1.25(–8)	$3s3p^3 3d\ ^6D^o$	774513 ± 600	(*)
45	7/2	773389	4.19(–9)	4.53(–9)	$3s3p^3 3d\ ^6D^o$	773389 ± 600	(*)
46	9/2	775182	3.04(–8)	2.87(–8)	$3s3p^3 3d\ ^6D^o$	775182 ± 600	(*)

These $3s^2 3p^3 - 3s3p^4$ lines are fairly intense in prompt spectra, and their differential longevity is clearly seen in spectra at 28 and 32 MeV ion energies, recorded at foil displacements of 1 mm (delay 100 ps), 2 mm, 5 mm, 10 mm and 20 mm. However, these lines (and most of the calibration lines which appear in the 32 MeV spectra) are near 30 nm and thus not close to the wavelength regions of interest for the decays of long-lived $J = 7/2$ levels (near 20 nm) or for the sextet levels (near 40 nm). Moreover, the sextet level decays by necessity have to be sought at ion energies below those suited for calibration with, say, Cu XIX $3s-3p-3d$ transitions. Calibrations based on wavelengths in prompt spectra are not necessarily transferable with notable precision to delayed spectra in such different wavelength ranges. However, it turns out that some of the wanted lines from sextet level decays are reasonably close to the intercombination ground state transitions in the Mg-, Al- and Si-like ions which had been identified earlier in similarly delayed beam-foil spectra [18–20]. Furthermore, in order to identify the sextet level decays, it is helpful to locate the positions of the levels they decay to, and that involves the $J = 7/2$ levels of the $3s^2 3p^2 3d$ configuration.

Fritzsche *et al.* [28,29] have presented extensive *ab initio* calculations of the Cl and P sequences, the wavelength predictions of which come closer to experiment than those of earlier calculations. For example, their level values for most of the Fe XII $3s^2 3p^2 3d$ levels are within about 1% of the experimentally known values. Cu, however, for which experimental conditions seemed most promising for identifying the long-lived decays, was not covered by that previous calculation. This gap has now been closed. The calculations predict two of the transitions from the long-lived Cu XV $J = 7/2$ levels at wavelengths of 20.534 nm and 21.097 nm and with upper level lifetimes of about 13.7 and 18.3 ns, respectively. Indeed, in delayed spectra recorded at positions up to 10 cm downbeam of the foil (delay times of order 10 ns), two lines, one on either side of the ground state intercombination transition array in the S-like spectrum, showed up more prominently with longer delay times, with wavelengths of 20.63 nm and 21.16 nm, respectively (Fig. 1). The decay curves yielded strong lifetime components of 11.4 ns for the one and 20 ns for the other line, corroborating the assignment with the wanted transitions in the P-like ion. While a weak third $J = 7/2$ level decay could also be localized in the spectra, there is another, fourth, level of J=7/2. Its lifetime has been predicted at more than 100 ns, which is too long for our experimental set-up. Furthermore, the low transition probability renders this decay too weak for our detection efficiency. However, it might show in astrophysical spectra.

This confirmation of the precision of the calculations for $J = 7/2$ levels in Cu XV permitted similar isoelectronic identifications in Ni XIV (one of the two lines being blended by an intercombination transition array in the S-like ions), Co XIII and Fe XII [17]. The latter is of particular interest because of the Fe abundance in the solar corona. Indeed, from the beam-foil spectra it was possible to identify lines in solar flare spectra [42,43]. As in preceding work on the Al isoelectronic sequence [19], the precision of the solar spectral wavelength data is much better than what could be achieved with the feeble, fast-beam light source. However, the isotopic purity and inherent time resolution make the foil-excited fast ion beam a unique tool for line identification. These observations fixed some of the missing $3s^2 3p^2 3d$ level energies within a few percent of the calculated data (Tab. 2). At the next step, candidate lines for the $3s3p^3 3d\ ^6D$ level decays have been found in the spectra of Cu, at positions which imply almost perfectly predicted $^6D^o$ level energies (Fig. 3). There are alternative positions for this multiplet at shorter wavelengths, but none at longer wavelengths. This stated agreement of prediction and observation for one group of levels does not imply that the full calculation is equally perfect. As stated above, the line assignment involved an empirical correction of the lower levels of this line multiplet. Also, there may be a fortuituous situation of a different kind: With the Cowan code regularly a systematic mismatch of *ab initio* calculated and measured level energies is observed that can be drastically improved by using a set of "standard" scaling values of the Slater parameters and certain integrals [25]. With some MCDF computations a different behaviour has been found, that is an overestimate of low and an underestimate of higher-lying levels, for example with Fe X [44] which is one of the most extensively (though incompletely) known term systems of solar physics interest [13]. In the range of crossover, the deviation of prediction and observation may be minimal. This might explain why our calculated sextet levels agree with experiment better than some lower lying levels.

Our Cowan code calculations show about the same general atomic structure situation for Ni. In fact, the earlier Bochum spectra on intercombination transitions in the Mg-, Al- and Si-like ions of iron group elements [18–20] cover the wavelength range of the sextet level decays in all those ions as well. In principle, we could derive information on the sextet level decays in P-like ions of other elements from those other data, too. However, with lower nuclear charge, the transition energies and rates are lower and the lifetimes much longer, spreading the decay curves even farther along the ion beam. Thus the signal from the sextet level decays will be weaker. While Ni can be produced as a strong ion beam, the next elements down in nuclear charge (Co, Fe, Mn) or up (Zn) can not, practically precluding such beam-foil observations at the present accelerator. In the solar corona, however, with time-integrated excitation and observation, this argument would not hold. Here the difficulty is that the population of the sextet levels is not known and may well be expected to be low.

Our data are unique in many ways, but they also demonstrate the advantage of and need for a systematic approach to the analysis of atomic spectra. Without a simultaneous analysis of several isoelectronic trends, there is little chance for progress with the study of the open $3d$ shell. Our wavelength (and lifetime) data are good enough to discriminate among several calculations. Although the overall pattern of spectral lines can be predicted, there often are notable differences of detail, like some lifetime

predictions which often are at variance with experience by about 30% and sometimes by factors of three.

The present MCDF calculations are much more extensive than those presented earlier [29], which in turn surpassed the early calculations by Huang [30]. While the basic relativistic approach is similar in all three calculations, either a judicious choice of wavefunctions or a massive scale, including a large number of CSF, seems to be needed to achieve accurate predictions.

The upkeep of the tandem accelerator and the provision of strong and stable ion beams by the Bochum crew of operators around K. Brand is gratefully acknowledged. Parts of this study were supported by Fysiografiska Selskap Lund, Deutsche Forschungsgemeinschaft (DFG), and an Exchange Program of Deutscher Akademischer Austauschdienst (DAAD) with Svenska Institutet (SI).

References

1. B. Edlén, Ark. Mat. Astr. Fys. B **28**, 1 (1941).
2. B. Edlén, Z. Astrophys. **22**, 30 (1942).
3. B. Edlén, R. Smitt, Solar Phys. **57**, 329 (1978).
4. K. Mori, M. Otsuka, T. Kato, *Grotrian Diagrams of Highly Ionized Iron, Fe VIII - Fe XVI* (Institute of Plasma Physics, Nagoya University, 1977).
5. R. Hutton, Jupén, Träbert, P.H. Heckmann, Nucl. Instrum. Meth. B **23**, 297 (1987).
6. J. Sugar, C. Corliss, J. Phys. Chem. Ref. Data **14**, Suppl. 2 (1988).
7. V. Kaufman, J. Sugar, W.L. Rowan, J. Opt. Soc. Am. B **6**, 1444 (1989).
8. V. Kaufman, J. Sugar, W.L. Rowan, J. Opt. Soc. Am. B **7**, 1169 (1990).
9. J. Sugar, V. Kaufman, J. Opt. Soc. Am. B **3**, 704 (1986).
10. J. Sugar, V. Kaufman, W.L. Rowan, J. Opt. Soc. Am. B **7**, 152 (1990).
11. J. Sugar, A. Musgrove, J. Phys. Chem. Ref. Data **19**, 527 (1990).
12. J. Sugar, V. Kaufman, W.L. Rowan, J. Opt. Soc. Am. B **8**, 22 (1991).
13. C. Jupén, R. Isler, E. Träbert, Mon. Not. R. Astr. Soc. **264**, 627 (1993).
14. T. Shirai, J. Sugar, W.L. Wiese, J. Phys. Chem. Ref. Data, Monograph **8** (1997), *Grotrian Diagrams for Highly Ionized Titanium (and other elements)*, JAERI-DATA/Code 97-022 to -031 (Japan Atomic Energy Research Institute, 1997).
15. NIST Atomic Spectroscopy Data Base / Astrophysics Data System, on-line data base at http://aeldata.nist.gov (January 1998).
16. U. Feldman, W.E. Behring, W. Curdt, U. Schühle, K. Wilhelm, P. Lemaire, T.M. Moran, Astrophys. J. Suppl. **113**, 195 (1997).
17. E. Träbert, Mon. Not. R. Astr. Soc. (in print 1998).
18. E. Träbert, R. Hutton, I. Martinson, Z. Phys. D **5**, 125 (1987).
19. E. Träbert, R. Hutton, I. Martinson, Mon. Not. R. astr. Soc. **227**, 27 (1987).
20. E. Träbert, P.H. Heckmann, R. Hutton, I. Martinson, J. Opt. Soc. Am. B **5**, 2173 (1988).
21. E. Träbert, M. Brandt, J. Doerfert, J. Granzow, P.H. Heckmann, J. Meurisch, I. Martinson, R. Hutton, R. Myrnäs, Physica Scripta **48**, 580 (1993)
22. E. Träbert, J. Doerfert, J. Granzow, P.H. Heckmann, C. Jupén, R. Hutton, E. Takács, Abstracts Vth Int. Coll. ASOSALP (Meudon France) 1995.
23. E. Träbert, J. Phys. B: At. Mol. Opt. Phys. **29**, L217 (1996).
24. Courtesy of C. Jupén.
25. R.D. Cowan, *The Theory of Atomic Structure and Spectra* (University of California Press, Berkeley, California, 1981).
26. E. Träbert, in *Accelerator-based Atomic Physics - Techniques and Applications*, edited by S.M. Shafroth and J.C. Austin (AIP Press, Washington 1997), p. 567
27. E. Träbert, Z. Phys. D **2**, 213 (1986).
28. S. Fritzsche, M. Finkbeiner, B. Fricke, W.-D. Sepp, Phys. Scr. **52**, 258 (1995).
29. S. Fritzsche, C. Froese Fischer, B. Fricke, At. Data Nucl. Data Tables **68**, 149 (1998).
30. K.-N. Huang, At. Data Nucl. Data Tables **30**, 313 (1984).
31. I.P. Grant, in *Methods in Comput. Chemistry*, vol. 2, edited by S. Wilson (Plenum Press, New York, 1988) p. 1.
32. F.A. Parpia, C. Froese Fischer, I.P. Grant, Comput. Phys. Commun. **94**, 249 (1996).
33. B.O. Roos, P.R. Taylor, P.E.M. Siegbahn, Chem. Phys. **48**, 157 (1980).
34. C. Froese Fischer, Phys. Scr. **49**, 323 (1994); M. Godefroid, J. Olsen, P. Jönsson, C. Froese Fischer, Ap. J. **450**, 473 (1995).
35. P.O. Löwdin, Phys. Rev. **97**, 1474 (1955).
36. S. Fritzsche, C. Froese Fischer, Comput. Phys. Commun. **99**, 323 (1997).
37. R.O. Sayer, Rev. de Phys. Appl. **12**, 1543 (1977).
38. K. Shima, N. Kuno, M. Yamanouchi, H. Tawara, At. Data Nucl. Data Tables 51, 173 (1992).
39. E. Träbert, H. Winter, P.H. Heckmann, H.v. Buttlar, Nucl. Instrum. Meth. **135**, 353 (1976).
40. E. Träbert, Phys. Scr. T **8**, 112 (1984).
41. E. Biémont, Phys. Scr. **33**, 324 (1986).
42. W.E. Behring, L. Cohen, U. Feldman, G.A. Doschek, Astrophys. J. **203**, 521 (1976).
43. K.P. Dere, Astrophys. J. **221**, 1062 (1978).
44. S. Fritzsche, C. Kohstall, (private communication 1998).